*Geophys. J. Int.* (2006) **165,** 658–667 doi: 10.1111/j.1365-246X.2006.02952.x

# Scattering of waves in elastic media containing passive and active cracks

Masatoshi Miyazawa[1] and Ichiro Nakanishi[2]

[1] *Disaster Prevention Research Institute, Kyoto University, Uji, Kyoto* 611-0011*, Japan. E-mail: linen@eqh.dpri.kyoto-u.ac.jp*
[2] *Department of Geophysics, Graduate School of Science, Kyoto University, Kyoto* 606-8502*, Japan*

Accepted 2006 February 3. Received 2006 February 2; in original form 2005 May 12

## SUMMARY

Scattering of wavefields in a 3-D medium that includes passive and/or active structures, is numerically solved by using the boundary integral equation method (BIEM). The passive structures are velocity anomalies that generate scattered waves upon incidence, and the active structures contain endogenous fracture sources, which are dynamically triggered by the dynamic load due to the incident waves. Simple models are adopted to represent these structures: passive cracks act as scatterers and active cracks as fracture sources. We form cracks using circular boundaries, which consist of many boundary elements. Scattering of elastic waves by the boundaries of passive cracks is treated as an exterior problem in BIEM. In the case of active cracks, both the exterior and interior problems need to be solved, because elastic waves are generated by fracturing with stress drop, and the growing crack boundaries scatter the incident waves from the outside of the cracks. The passive cracks and/or active cracks are randomly distributed in an infinite homogeneous elastic medium. Calculations of the complete waveform considering a single scatter show that the active crack has weak influence on the attenuation of first arrivals but strong influence on the amplitudes of coda waves, as compared with those due to the passive crack. In the active structures, multiple scattering between cracks and the waves triggered by fracturing strongly affect the amplitudes of first arrivals and coda waves. Compared to the case of the passive structures, the attenuation of initial phase is weak and the coda amplitudes decrease slowly.

**Key words:** crack media, fault slip, scattering, seismic coda.



## 1 INTRODUCTION

The Earth's lithosphere is made of active and passive structures, which are characterized by the release and the non-release of strain energy, respectively (Rykunov *et al.* 1979; Nikolaev & Troitskiy 1987). Seismic waves propagating through the passive structure are affected by the attenuation due to scattering and intrinsic absorption, but the waves passing through the active structure trigger strain energy due to endogenous sources, as acoustic emission in response to the induced dynamic stress changes (e.g. Diakonov *et al.* 1990; Privalovskiy & Beresnev 1994).

Some studies (Vinnik 1989; Galperin *et al.* 1990) suggest that such active structure, as discussed above, may not exist. For example, Nikolaev & Troitskiy (1987) have found steady seismic emission from a depth of about 100 km beneath the NORSAR, although Vinnik (1989) insists that their results must be caused by their wrong analysis of random fluctuation of traveltimes. Galperin *et al.* (1990) also show a negative evidence against short-period seismic emission from the active structure.

The phenomena attributed to the active structure include not only acoustic emission but also earthquakes triggered by stress changes (e.g. Harris 1998). Earthquakes triggered by seismic waves have been reported relatively recently (e.g. Hill *et al.* 1993; Kilb *et al.* 2000; Iwata & Nakanishi 2004; Miyazawa & Mori 2005; Miyazawa *et al.* 2005).

In order to investigate the possible nature of active structure, we assume, first, plausible generic methods to represent both passive and active structures, and calculate their complete seismic wavefields upon incidence. We choose static circular cracks for purely passive structure, and dynamic cracks for the purely active. We refer to the former cracks as passive cracks and the latter as active cracks.

The seismic scattering due to passive cracks has been studied by using analytical methods (e.g. Pao & Mow 1973; Achenbach *et al.* 1982) and by numerical methods (e.g. Nishimura & Kobayashi 1989; Murai *et al.* 1995; Yomogida & Benites 2002). Pao & Mow (1973) have obtained an exact solution of the displacement on the boundary of an inclusion embedded in elastic media. Using the boundary integral equation method (BIEM), Nishimura & Kobayashi (1989) have solved the elastodynamic crack problems. Yomogida & Benites (2002) have calculated the waves multiply scattered by dry cracks. The simulations of wavefields perturbed by fluid-filled cracks have been treated by Murai *et al.* (1995).

An example of an active crack is a fracture. Some problems of quasi-dynamical fracturing have been solved by analytical methods (e.g. Sato & Hirasawa 1973; Dahlen 1974; Sato 1994) and problems of kinematical and dynamical fracturing by numerical methods (e.g. Das 1980; Das & Kostrov 1987; Fukuyama & Madariaga 1998). These numerical methods often use BIEM, in which complicated boundary elements and conditions can be incorporated (Kame & Yamashita 1999; Aochi *et al.* 2002).

Our active structure consists of passive and active cracks, so that the scattering and fracturing problems are mutually related. In this study, we use the boundary integral equation derived by Kobayashi (1987, 2000) to express such interaction, distributing the passive and active cracks in a 3-D infinite elastic medium, and applying the BIEM to calculate the scattering of elastic waves.

## 2 BOUNDARY INTEGRAL EQUATION METHOD FOR PASSIVE AND ACTIVE CRACKS

### 2.1 Boundary integral equation

In BIEM the fracturing of a crack and the scattering by a crack are treated as an exterior problem and an interior problem, where we numerically calculate the exterior solution and the interior solution for the outside and inside of the crack boundaries $\partial D$, respectively (Fig. 1). The wave solution for the passive crack is represented by the exterior solution and we call it as 'a passive crack solution'. The perturbation of wavefield by the active crack that is 'an active crack solution', involves both interior and exterior problems. Using the boundary integral equation derived by Kobayashi (1987, 2000), we can solve simultaneously the exterior and interior problems in 3-D, to obtain the wavefield in the structure including passive and active cracks.

We consider the Cartesian domain $D$ and its boundary $\partial D$ in an ordinary 3-D space (Fig. 1). We use vector $\boldsymbol{x}$ to indicate the location $(x_1, x_2, x_3)$ and the normal vector $\boldsymbol{n}$ to $\partial D$, defined as positive when it points towards the outside of $D$. The displacement vector $\boldsymbol{u}$ and the traction vector $\boldsymbol{t}$ are a function of $\boldsymbol{x}$ and the time $t$, while $\hat{\cdot}$ stands for the vector in the domain of the angular frequency $\omega$. $\hat{\boldsymbol{u}}(\boldsymbol{x};\omega)$ at

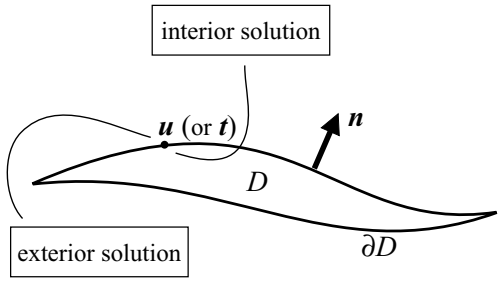


passive crack solution = exterior solution
active crack solution = interior & exterior solutions

**Figure 1.** Interior and exterior problems for a crack bounded by $\partial D$. $\boldsymbol{n}$ is normal vector to $\partial D$. Interior and exterior problems consider the interior and exterior sides of the boundary, respectively. The solution $\boldsymbol{u}$ (or $\boldsymbol{t}$) on $\partial D$ is obtained in both problems. If we consider the wavefield out of the boundary, which is a scattering problem by a passive crack, we have the exterior solution (a passive crack solution). The interior solution is the fracturing of an active crack in this study. Then, for the scattering wavefield by the active crack, we need both interior and exterior solutions (an active crack solution).

any point $\boldsymbol{x}$ off $\partial D$ is written by means of the integral representation theorem in the frequency domain, as (Kobayashi 1987)

$$\epsilon(\boldsymbol{x})\hat{u}_i(\boldsymbol{x};\omega) = \int_{\partial D} [\hat{U}_{ik}(\boldsymbol{x},\boldsymbol{y};\omega)\hat{t}_k(\boldsymbol{y};\omega) - \hat{W}_{ik}(\boldsymbol{x},\boldsymbol{y};\omega)\hat{u}_k(\boldsymbol{y};\omega)]\, ds(\boldsymbol{y}) \qquad i,k = 1,2,3 \tag{1}$$

$$\epsilon(\boldsymbol{x}) = \begin{cases} 1, & \boldsymbol{x} \in D \\ 0, & \boldsymbol{x} \in D_c \end{cases}, \tag{2}$$

where $\hat{\boldsymbol{U}}(\boldsymbol{x},\boldsymbol{y};\omega)$ is the fundamental solution for a station at $\boldsymbol{x}$ and a source at $\boldsymbol{y}$ and $\hat{\boldsymbol{W}}(\boldsymbol{x},\boldsymbol{y};\omega)$ is the double layer potential kernel, meaning the traction at a station $\boldsymbol{y}$ for a source at $\boldsymbol{x}$, and $D_c$ the complement of $D$. The fundamental solutions, $\hat{\boldsymbol{U}}(\boldsymbol{x},\boldsymbol{y};\omega)$ and $\hat{\boldsymbol{W}}(\boldsymbol{x},\boldsymbol{y};\omega)$, are explicitly given (e.g. Eringen & Suhubi 1975; Kupradze 1979; Kobayashi 1987).

We consider the case that the station $\boldsymbol{x}$ is infinitesimally close to the boundary. Using limit properties of the potentials, we have a boundary integral equation (Kobayashi 1987)

$$C^+_{ik}(\boldsymbol{x})\hat{u}_k(\boldsymbol{x};\omega) = \int_{\partial D} \hat{U}_{ik}(\boldsymbol{x},\boldsymbol{y};\omega)\hat{t}_k(\boldsymbol{y};\omega)\, ds(\boldsymbol{y}) - \hskip-1em \int_{\partial D} \hat{W}_{ik}(\boldsymbol{x},\boldsymbol{y};\omega)\hat{u}_k(\boldsymbol{y};\omega)\, ds(\boldsymbol{y}), \tag{3}$$

where $f()ds$ implies the Cauchy principal value integral and $C^+_{ik}(\boldsymbol{x})$ is $\delta_{ik}$ for $\boldsymbol{x} \in D$ and $\delta_{ik}/2$ for $\boldsymbol{x} \in \partial D$ if the boundary in contact with $\boldsymbol{x}$ is smooth. The first integral term and the second term, are called the single layer potential and the double layer potential, respectively. For a numerical calculation of the double layer potential, some regularization is required to evaluate the principal value integral with singularity. We discretize the boundary integral equations by assigning the values of displacements and tractions to the nodes of boundary elements. To remove and reduce the influence of the singularity, we use an interstand remeshing method (Beskos 1987), which replaces a non-triangular boundary element with a triangular element $ds$, so that $ds$ is transformed into $rdrd\theta$ in polar coordinates. When $r = |\boldsymbol{x} - \boldsymbol{y}| \to 0$, the two fundamental solutions have singularities $\hat{U}$ of $O(1/r)$ and $\hat{W}$ of $O(1/r^2)$. However, with the interstand remeshing method, the first integral term in eq. (3) has no singularity and the singularities of the second integral can be reduced to $O(1/r)$. By solving eq. (3) with initial conditions, we have the displacement $\hat{\boldsymbol{u}}(\boldsymbol{x};\omega)$ and the traction $\hat{\boldsymbol{t}}(\boldsymbol{x};\omega)$ on the boundary.

Eq. (3) shows the interior program in $D$. When we consider the exterior area of $D$ and there is no affect from the far-field (a radiation condition), the interior representation (3) can be applied to the exterior (Kitahara 1985). The scattered wavefield satisfies the radiation condition. We can write the scattered wavefield $\hat{\boldsymbol{u}}^{\rm sc}(\boldsymbol{x};\omega)$ as

$$\hat{\boldsymbol{u}}^{\rm sc}(\boldsymbol{x};\omega) = \hat{\boldsymbol{u}}(\boldsymbol{x};\omega) - \hat{\boldsymbol{u}}^{\rm in}(\boldsymbol{x};\omega), \tag{4}$$

where $\hat{\boldsymbol{u}}$ is total wavefield and $\hat{\boldsymbol{u}}^{\rm in}$ is incident wavefield. Similarly,

$$\hat{\boldsymbol{t}}^{\rm sc}(\boldsymbol{x};\omega) = \hat{\boldsymbol{t}}(\boldsymbol{x};\omega) - \hat{\boldsymbol{t}}^{\rm in}(\boldsymbol{x};\omega). \tag{5}$$

We have the equations for the exterior problems by substituting $\hat{\boldsymbol{u}}^{\rm sc}$ and $\hat{\boldsymbol{t}}^{\rm sc}$ for $\hat{\boldsymbol{u}}$ and $\hat{\boldsymbol{t}}$, respectively, in eqs (1) and (3). Once the boundary integral eq. (3) is solved, we can calculate the wavefield at any point $\boldsymbol{x}$ in $D$ from the representation theorem (1) with the solutions of displacement $\hat{\boldsymbol{u}}$ and traction $\hat{\boldsymbol{t}}$ on the boundaries.

The crack fracturing and the scattering by one side of the crack surface can be represented by eqs (1)–(3). To calculate the multiple scattering wavefield by the passive crack, the exterior problem of

a crack bounded by two planes without the complement domain requires a representation different from the above.

For a crack with free surface $S$, the displacement vector off $S$ is

$$\hat{\boldsymbol{u}}(\boldsymbol{x};\omega) = \hat{\boldsymbol{u}}^{\text{in}}(\boldsymbol{x};\omega) + \int_S \hat{\boldsymbol{W}}(\boldsymbol{x},\boldsymbol{y};\omega)\Delta\hat{\boldsymbol{u}}(\boldsymbol{y};\omega)\,ds, \tag{6}$$

where $\Delta\hat{\boldsymbol{u}}$ is a dislocation of displacement across the crack surface. The limit properties of the potentials yield the boundary integral equation (Nishimura & Kobayashi 1987)

$$-\overset{\boldsymbol{n}}{\boldsymbol{T}}\,\hat{\boldsymbol{u}}^{\text{in}}(\boldsymbol{x};\omega) = \text{p.f.}\int_S \overset{\boldsymbol{n}}{\boldsymbol{T}}\,\hat{\boldsymbol{W}}(\boldsymbol{x},\boldsymbol{y};\omega)\Delta\hat{\boldsymbol{u}}(\boldsymbol{y};\omega)\,ds, \tag{7}$$

where $\overset{\boldsymbol{n}}{\boldsymbol{T}}$ is the elastic traction operator defined as

$$\hat{W}_{ki}(\boldsymbol{x},\boldsymbol{y};\omega) = \overset{n(\boldsymbol{y})}{T}_{ij}\,\hat{U}_{kj}(\boldsymbol{x},\boldsymbol{y};\omega), \tag{8}$$

p.f. designates the finite part of the divergent integral and the boundary condition includes no dislocation at the crack tip (Nishimura & Kobayashi 1989). This boundary integral equation has a (hyper-) singularity (Tanaka *et al.* 1994).

### 2.2 Accuracy and stability of the solution

Hereafter, we use $(x, y, z)$ instead of $(x_1, x_2, x_3)$.

#### *2.2.1 Interior problem*

An example of the interior problem is a crack fracturing in a plane (Fig. 2). The boundary $S$ is divided into two regions, $S_1$ and $S_2$, where only the region $S_1$ will fracture. On $S_1$, the stress drop associated with the fracture is given *a priori*, so that the traction $\hat{\boldsymbol{t}}$ is known, while on $S_2$ no displacement ($\Delta\hat{\boldsymbol{u}} = \boldsymbol{0}$) is given because there is no fracture (Table 1). Solving eq. (3), we have the solution that shows the slip $\Delta\boldsymbol{u}$ ($=\boldsymbol{u}$, in this case) on $S_1$ and the traction $\boldsymbol{t}$ on $S_2$.

We test our BIEM code by solving a kinematic crack problem. The rupture of a plane crack including a self-similar nucleation is analytically solved (e.g. Sato & Hirasawa 1973; Dahlen 1974; Sato 1994). We compare our numerical solutions with the corresponding analytical solutions, assuming that the rupture starts at the centre of a circular crack with the crack boundary moving towards the positive $x$. We also assume that the stress drop is $\Delta\sigma$ (Table 1). The rupture velocities in the directions $x$ and $y$ are $v_x = c_T$ (shear wave velocity) and $v_y = c_R$ (Rayleigh wave velocity), respectively, where the ruptured surface includes neither friction nor cohesion and the maximum rupture velocities are expected: shear wave velocity for mode-II and Rayleigh wave velocity for mode-III (Richards 1973; Dahlen 1974). In our finite crack model we assume that the region beyond the circular crack with radius $a$ is a barrier with effective infinite strength. In the kinematic problem, the rupture velocity is given and the whole crack boundary is assumed to rupture with the given stress drop. The time histories of $\boldsymbol{t}$ (and $\hat{\boldsymbol{t}}$ in the frequency domain) should be given *a priori* on $S$, therefore, we need not consider $S_2$ but only $S_1$ in the calculation. Boundary elements are generated by the method of Everett (1997), illustrated in Fig. 3, where triangular elements are adopted for the use of the interstand remeshing method.

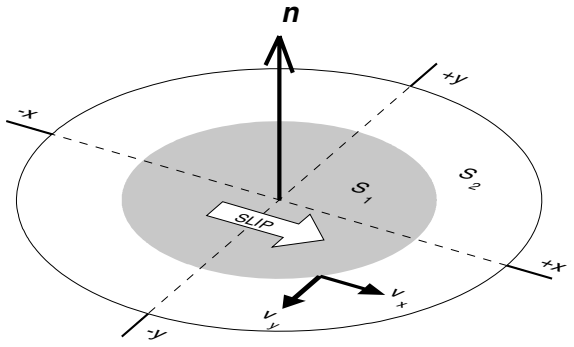


**Figure 2.** Spontaneously fracturing crack. One side of the crack boundary is illustrated and the boundary is plane with normal vector $\boldsymbol{n}$. The boundary consists of two parts, $S_1$ and $S_2$, where the boundary will be fractured and not, respectively. The white arrow toward $+x$ indicates the slip direction on this side. The slip direction of the opposite side is $-x$. $v_x$ and $v_y$ are the rupture velocities in the $x$- and $y$-direction, respectively.

**Table 1.** Boundary condition of a crack in the time domain.

| | Known | Unknown |
|---|---|---|
| $S_1$: fractured region | $\Delta\boldsymbol{u}\,\vert_y = \Delta\boldsymbol{u}\,\vert_z = 0$<br>(stress change in $\boldsymbol{t}\,\vert_x$) $= -\,\Delta\sigma$<br>$\boldsymbol{t}\,\vert_y = \boldsymbol{t}\,\vert_z = 0$ | $\Delta\boldsymbol{u}\,\vert_x$ |
| $S_2$: non-fractured region | $\Delta\boldsymbol{u} = \boldsymbol{0}$ | $\boldsymbol{t}$ |

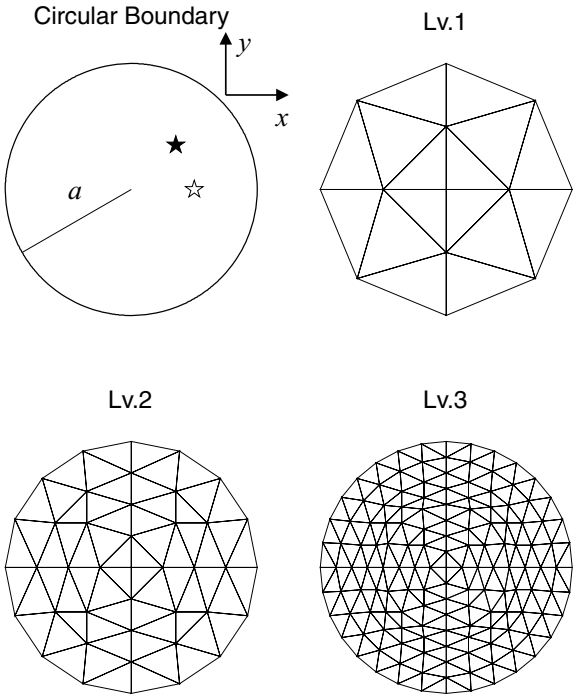


**Figure 3.** Boundary elements for a plane circular crack. Circular boundary of radius $a$ (top left) is divided into triangular boundary elements by the method of Everett (1997). Large index Lv. indicates fine boundary elements meshes. Lv. 1: 16 elements and 13 nodes, Lv. 2: 64 elements and 41 nodes and Lv. 3: 256 elements and 145 nodes. Two stars on the crack are the points where the slip histories are shown in Fig. 4.

Fig. 4 shows the time-domain comparison of the slip functions on the boundary, obtained by the BIEM, with those by the quasi-dynamic method (Sato 1994). During the rupture propagation, both slip functions are in agreement with each other. The crack in the quasi-dynamic method continues to slip because of the infinite crack plane, while that in the BIEM stops the slip after the rupture front arrives at the barrier. The final slip in the BIEM depends on the sizes

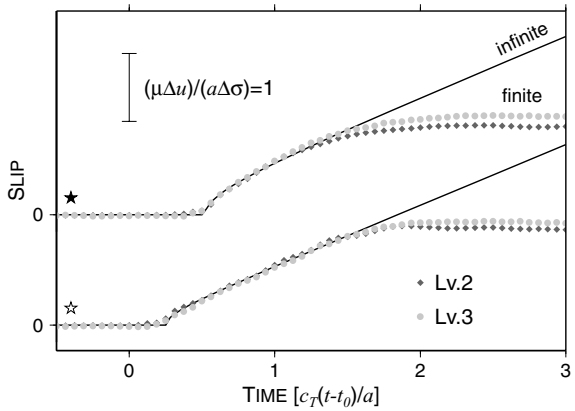


**Figure 4.** Slip functions of the kinematic circular crack at the two points indicated in Fig. 3. The circular crack begins to rupture at time $t = t_0$ from the central point with the rupture velocity of $v_x = c_T$ (shear wave velocity) and $v_y = c_R$ (Rayleigh wave velocity). We assume $c_R/c_T = 0.9194$. Solid lines are quasi-dynamic solutions (Sato 1994), and diamonds and circles are solutions by BIEM using different meshes Lv. 2 and Lv. 3 (Fig. 3). Time and slip are normalized. $\mu$ is rigidity, $\Delta u$ slip displacement and $\Delta\sigma$ stress drop.

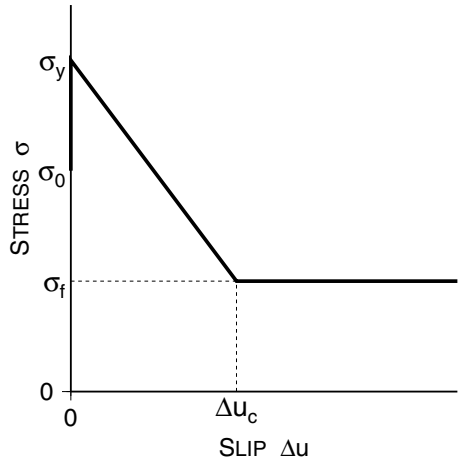


**Figure 6.** Constitutive relation between the slip and friction condition required by slip-weakening law. The friction is initially $\sigma_0$. Once the stress reaches $\sigma_y$, the slip starts and the friction gradually decreases. When the slip reaches a certain yield limit $\Delta u_c$, the friction continues to take a constant level $\sigma_f$.

of the boundary elements (Lv. 2 or Lv. 3 in Fig. 3). However, the differences of the final slip are slight and the numerical calculation is stable.

We apply the BIEM to the dynamic circular crack problem, in which the rupture spontaneously propagates with admissible velocity under friction. The initial conditions on the crack are shown in Fig. 5. The central area of the crack is a brittle circular region of radius $a/4$, where high stress drop is expected. At time $t = t_0$ we raise the initial stress $\sigma_0$ at the brittle region to the same level as the yield stress $\sigma_y$, then the rupture of the crack starts. The rupture growth is influenced by the slip-weakening law (Andrews 1976) (Fig. 6). If the traction at an arbitrary point on $S_2$, which is defined by $r > a/4$, exceeds the threshold to rupture, the rupture starts there. Then the traction and the boundary condition on $S_2$ determine the rupture velocities and the fractured point is included in $S_1$. We solve for the slip and the traction enlarging $S_1$ and reducing $S_2$, and iterate the procedure until the rupture condition is no longer provided or $S_2$ has no area. When the rupture front arrives at crack tip $r = a$, where the yield stress is supposed to be infinite (i.e. barrier), the rupture on the boundary stops. Fig. 7 shows the slip function at the centre of the crack for different critical slip $\Delta u_c$, which is the yield limit for the stress to drop to a constant $\sigma_f$. Slip rate (or slip velocity) slowly increases for large $\Delta u_c$ and reaches a similar rate in every case, thereby suggesting the slip delay. The final slip and rupture velocities decrease with $\Delta u_c$. The rupture velocities are about 50 per cent of the shear wave velocity $c_T$ and $v_x > v_y$. The result obtained in our calculation is consistent with the result of Fukuyama & Madariaga (1998), who showed the slip velocity, the slip and the stress on circular faults by changing $\Delta u_c$ with the slip-weakening or rate-weakening friction lows.

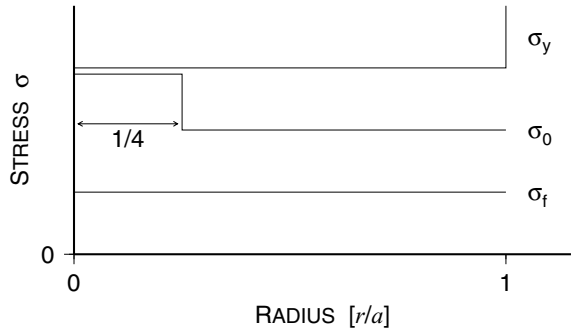


**Figure 5.** Stress condition on a circular crack. $\sigma_0$ is initial stress, $\sigma_f$ is friction stress and $\sigma_y$ is yield stress. The central area of radius $a/4$ is a brittle circular region, where the initial stress and the stress drop are higher than the other area. At the crack tip $r = a$, barrier is supposed by taking infinite $\sigma_y$.

### *2.2.2 Scattering by a passive crack*

The BIEM is applied to a simple example to obtain a passive crack solution. One circular crack is located in a full-space elastic medium, where Poisson's ratio $\nu = 0.25$. The boundary elements are Lv.2 in Fig. 3. We obtain the scattering cross-section normalized by the crack surface area $\pi a^2$, for the normal incidence of a monochromatic plane $P$ wave with wavenumber $k$, where $a$ is the radius of the crack (Fig. 8). The solution by the BIEM is in an agreement with the solution given by Martin & Wickham (1983).

## 2.3 Scattering problem for an active crack

In the case of scattering problem for an active crack, the incident wave dynamically triggers the rupture of the active crack and the spontaneously growing crack boundary scatters the wave (Fig. 9).

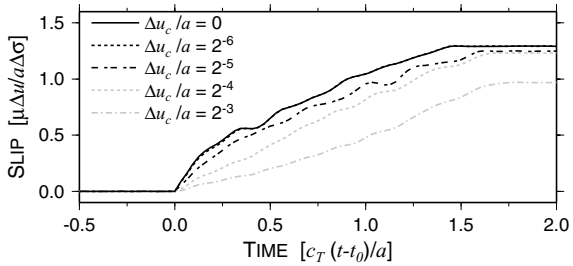


**Figure 7.** Slips on the centre of circular crack for $\Delta u_c$. Plane circular crack boundaries of Lv. 3 in Fig. 3 are used. We suppose $\sigma_y/\mu = 0.3$, $\sigma_f/\mu = 0.1$ and $\sigma_0/\mu = 0.2$ for $a/4 < r$ (see Figs 5 and 6). The fracture starts at time $t = t_0$ from the brittle region.

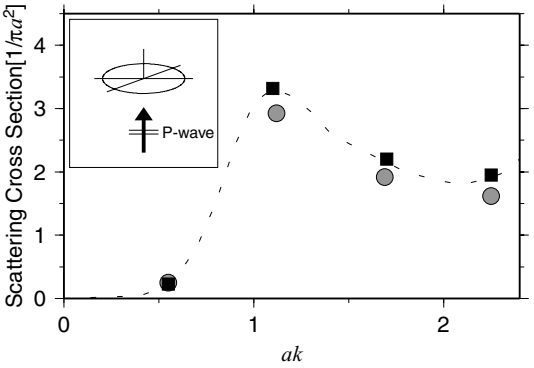


**Figure 8.** Scattering cross-section of a passive crack for $ak$. Incident plane $P$ wave with wavenumber $k$ is vertical to the surface of the crack with radius $a$ as indicated in the inset figure. Squares with a dotted line are solution by BIEM and circles are by Martin & Wickham (1983).

Then the interior and exterior problems are mutually related in the calculation of the wavefield (Figs 1 and 9). The solutions of the boundary integral equations in both problems are the displacements and tractions. Hence, we can easily combine the two problems to obtain the active crack solution. In the boundary integral equation of the exterior problem for the active crack, we assume that the non-fractured area has no potential, that is, neither the single layer nor the double layer potential. The incident waves are scattered by the fractured area of the crack.

## 3 WAVEFIELDS GENERATED BY PASSIVE AND/OR ACTIVE CRACKS

We calculate the response of the elastic media containing passive and/or active cracks to the incidence of a plane $S$ wave. All the cracks have a constant radius $a$ and are distributed randomly. The Ricker wavelet (Ricker 1945) with dominant frequency $f$ which has the wavenumber $k$, and polarization in the $x$-direction, is used as the source time function, incident either on a single crack or on a group of cracks from the $z$-direction (Figs 9 and 10).

### 3.1 Single scattering by a passive crack and an active crack

The passive crack produces scattering upon incidence, while the active crack both, produces scattering and also radiates elastic waves by rupture, due to dynamic triggering (Fig. 9). Thus, the wavefield caused by the active crack is much complicated as compared with that by the passive crack. We calculate the wavefields for two cases in which either a passive crack or an active crack is located in an infinite elastic medium. We assume $ak = 3$ and show no direct wave propagation behind the crack and diffracted waves at the crack tip.

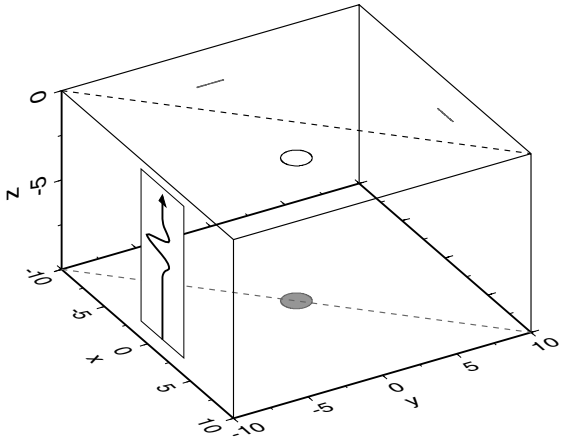


**Figure 10.** Location of one circular crack in an infinite elastic medium. The crack (open circle) of $ak = 3$ is either the passive crack or the active crack, and its surface is oriented horizontally and also shown are the projection on $xy$-, $yz$- and $zx$-planes. Broken line at $z = 0$ is a profile line, where stations are located to see the calculated displacements. Incident plane $S$ wave (Ricker wavelet) polarizing in $x$-direction and propagating through $+z$-direction, is shown on the $zx$-plane.

The boundary elements of Lv. 2 are used (Fig. 3). The properties of the active crack are the same as in Figs 5 and 6, where we assume that the slip direction is $+x$ on the lower boundary, $\Delta u_c = 0$ and $\sigma_f = 0$, which means that the fractured area is free surface. The traction of the crack boundary has a finite initial value $\Delta\sigma$ and drops to 0 after the fracture. The active crack becomes finally the passive crack. Fig. 10 shows the location of the crack, either passive or active, and the diagonal line along which observation points are selected.

Fig. 11(a) shows the calculated waveforms of the three-component displacements at the observation line for the case of the passive crack. The dimensions of the length and time are normalized by $a/3$ and $a/3c_T$, respectively. At the stations above the passive crack, the direct waves are weak because of no direct propagation through the crack. The waves due to diffraction around the crack tip follow the direct waves.

Fig. 11(b) shows the calculated waveforms for the active crack. When the traction acting on the brittle region exceeds the threshold $\sigma_y$, rupture is triggered and elastic waves are radiated. Then, the fractured region of the active crack immediately becomes passive. The total wavefield includes the elastic waves radiated by the rupture, which appear right after the direct wave. The amplitudes of the direct waves at the stations above the active crack (Fig. 11b) are not as attenuated as for the case of the passive crack (Fig. 11a). The scattering of waves due to the growing crack boundary is shown in Fig. 11(c), in which the wavefield due to the rupture has been

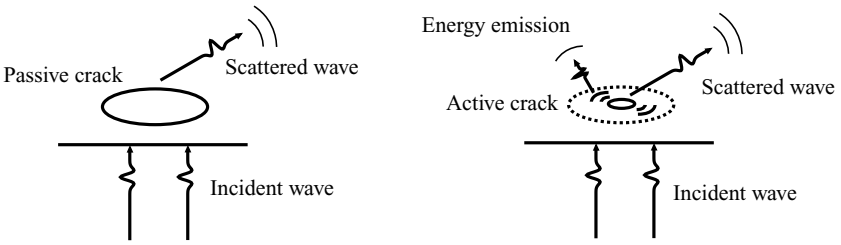


**Figure 9.** Schematic representation of a passive crack and an active crack. A plane wave is incident on the cracks. The passive crack generates scattered waves as secondary waves. The active crack generates scattered waves and other waves due to the rupture of the crack.

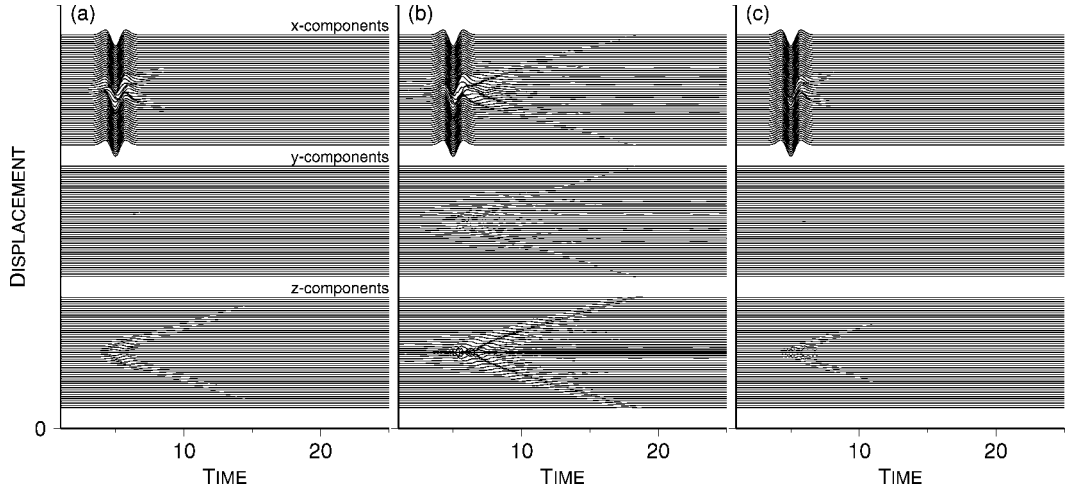


**Figure 11.** Calculated displacements due to the vertical incidence of a plane $S$ wave for the model of Fig. 10. The shape of the incident wave is Ricker wavelet and polarizes to $x$-direction ($t = 0$, $z = -5$). The length and time are normalized by $a/3$ and $a/3c_T$, respectively. (a) A model of one passive crack. The $x$-, $y$- and $z$-components of displacements are indicated. The observation points are set on the diagonal line from (10, 10, 0) to ($-10$, $-10$, 0) (Fig. 10) and the waveforms at the observation points are shown from the top to the bottom for each component. (b) A model of one active crack. Crack surface on the lower side slips to $+x$-direction. The fractured area is assumed to be free of traction. In the brittle region defined as $r \leq a/4$, $\Delta\sigma/\mu = 0.1$, $|\sigma_y - \sigma_0|/\Delta\sigma = 0.1$ and $\sigma_0 = 2\sigma_0|_{a/4<r<a}$. (c) A model of one active crack without radiation of energy due to the fracturing. The fractured area is assumed to be free of traction.

removed. At the stations above, the amplitudes of the direct waves are not as attenuated as in the case of the passive crack (Fig. 11a). This is because, when the initial phase of the incident wave arrives at the active crack, this does not rupture yet, hence, does not scatter the incident wave because there is no growing crack surface. Once the rupture starts due to dynamic triggering, the incident wave is scattered by the growing crack surface made by the rupture. The purity scattered wavefield is weak compared with that of the passive crack, until the rupture front reaches the radius $a$. Thus, in the active crack model (Fig. 11b), the amplitude of the first arrival depends on this weak scattering, the stress drop and the rupture start time.

### 3.2 Multiple scattering by passive cracks and active cracks

We calculate the wavefields perturbed by the two kinds of cracks distributed randomly in an elastic full-space. All the cracks are neither overlapped nor extremely close to each other. Multiple scattering between cracks plays an important role in scattering of elastic waves for dense distribution of cracks (Frankel & Clayton 1986; Yomogida & Benites 1995) and is formulated for use of the BIEM in this paper. The boundary elements of Lv. 1 and Lv. 2 (Fig. 3) are used for passive and active cracks, respectively. There is little difference between the cases of Lv. 1 and Lv. 2 to calculate the waves scattered by a passive crack.

Fig. 12 shows a random distribution of 25 passive cracks and 1 active crack used in the following examples. In the first, we will try to model the passive structure and consider only 25 passive cracks. Fig. 13(a) shows the three-component displacements calculated for the vertical incidence of a plane $S$ wave with $ak = 1.27$, which can provide the dominant scattering because strong scattering is expected when $ak \sim 1$ (e.g. Sato & Fehler 1998). There is a possibility of a scattering of a $P$ wave converted from the $S$ wave, where $ak_p = 0.73$ for the wavenumber $k_p$ of the $P$ wave, so that for any elastic waves, which have wavenumber $k_0$, we can expect $ak_0 \sim 1$ in this

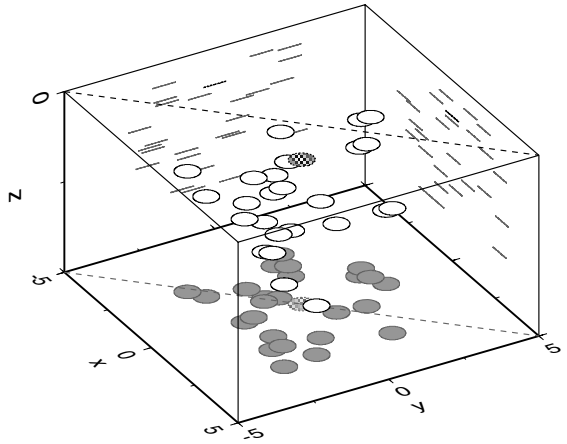


**Figure 12.** Distribution of 26 circular cracks ($ak = 1.27$) in an infinite elastic medium. Open circles are 25 passive cracks, while a circle filled with oblique lines is an active crack. All the cracks are randomly and laterally distributed and are projected on $xy$-, $yz$- and $zx$-planes. The broken line at $z = 0$ is the profile line.

model. The length and time are normalized by $a/1.27$ and $a/1.27c_T$, respectively. The scattered waves that result from multiply reflected and diffracted waves, make coda after the arrival of direct wave.

In the next example, an active crack is located among the 25 passive cracks (Fig. 12). For this, we have to solve the interior problem for the active crack, simultaneously with the exterior problem. The calculated waveforms (Fig. 13b) show strong coda, compared with the case of only passive cracks (Fig. 13a). To make this evident we take the differences of waveforms between Figs 13(a) and (b) and point it in Fig. 13(c). The radiated waves from the rupture of the active crack and their multiply scattered waves conform the coda, exhibiting large amplitudes.

Next, we add four active cracks to the model of Fig. 12 (Fig. 14a). The calculated waveforms show strong coda waves (Fig. 14b) due

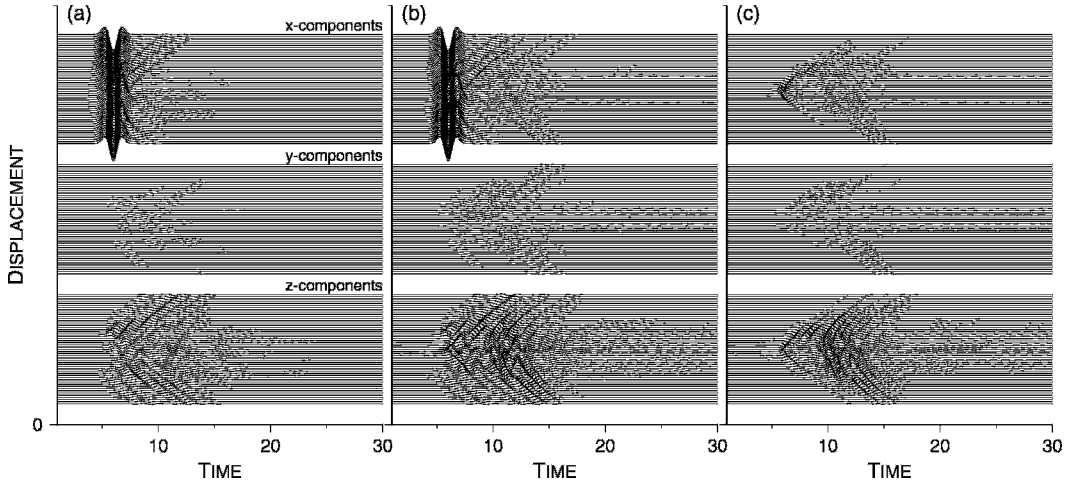


**Figure 13.** (a) Calculated displacements for the model considering the 25 passive cracks but not the active crack. The incident plane $S$ wave is generated toward $+z$-direction at $t = 0$ and $z = -6$. The three components of displacements on the profile line are shown. The waveforms on the profile line from (5, 5, 0) to $(-5, -5, 0)$ are shown from the top to the bottom for each component. The length and time are normalized by $a/1.27$ and $a/1.27c_T$, respectively. (b) Calculated displacements for the model of 25 passive cracks and one active crack. The model of Fig. 12 is used. The incident wave is the same as in (a). In the active crack, $|\sigma_y - \sigma_0|/\Delta\sigma = 0.05$ and $\Delta\sigma/\mu = 0.1$ for the brittle region ($r \leq a/4$) and $|\sigma_y - \sigma_0|/\Delta\sigma = 1$ and $\Delta\sigma/\mu = 0.05$ for the outside. The crack surface on the lower side slips to $+x$-direction. (c) Differences of the two wavefields for the model with 25 passive cracks (a) and that with 25 passive cracks and one active crack (b). The wavefield is obtained by subtracting traces of (a) from those of (b).

to wave contribution of the five active cracks. First arrival $P$ waves are observed in $z$-components (Fig. 14a).

The strong coda waves observed for the models containing active cracks cannot be generated by 40 passive cracks (Fig. 15).

### 3.3 Scattering attenuation

Scattering attenuation $Q^{-1}$ of the direct wave is calculated by measuring the attenuation of initial phase of the envelope. Changing the dominant wavenumber $k$ of the incident wave, we obtain the scattering attenuation $Q^{-1}$ as a function of $ak$ for the model of 25 passive cracks, in order to see whether or not our solutions in the passive structures are accurate. In Fig. 16, our $Q^{-1}$ is compared with $Q^{-1}$ from two single scattering models (Wu 1982). To calculate $Q^{-1}$ much precisely in the case of $ak = 0.32$, we need other crack distribution model with a long travel distance through cracks. It is believed that the scattering $Q^{-1}$ has a peak around $ak \sim 1$ (e.g. Kawahara & Yamashita 1992; Sato & Fehler 1998), with which our results are consistent.

### 3.4 Root-mean-square (rms) envelopes

We obtain the rms envelopes of velocity waveforms calculated for the 441 observation points at $z = 0$ for the four models of passive and active structures above. The coda amplitude increases with the increase of the number of passive cracks or active cracks (Fig. 17). The rms envelope in Fig. 17(b) (25 passive cracks and 1 active crack) shows that the coda amplitude becomes larger than that in the case of only passive cracks (Fig. 17a). For the model of 25 passive crack and 5 active cracks, the attenuation of the direct wave is a little smaller than the former two models (Figs 17a–c). In the model of 40 passive cracks, the amplitude of direct wave is much reduced and the amplitude of the coda is increased as compared with the case of 25 passive cracks (Figs 17a and d). However, in both cases, the constant total energy in the wavefield restricts the amplitude of the

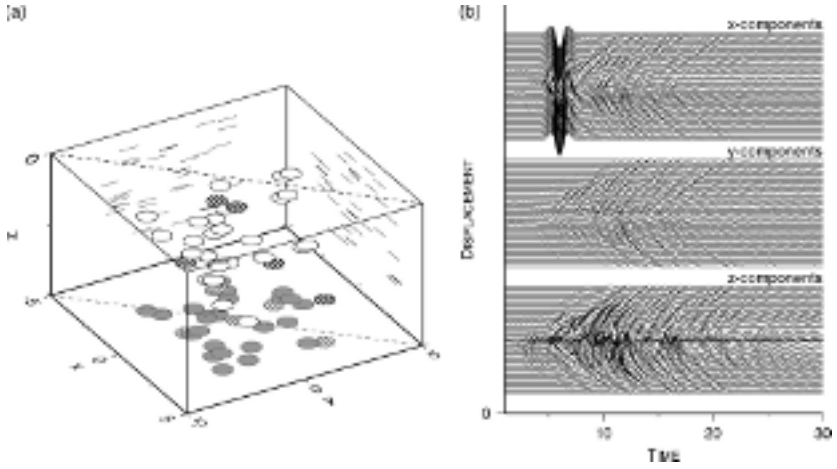


**Figure 14.** (a) Distribution of 25 passive cracks and 5 active cracks in infinite elastic medium. (b) Calculated displacements at the observation points on the profile line.

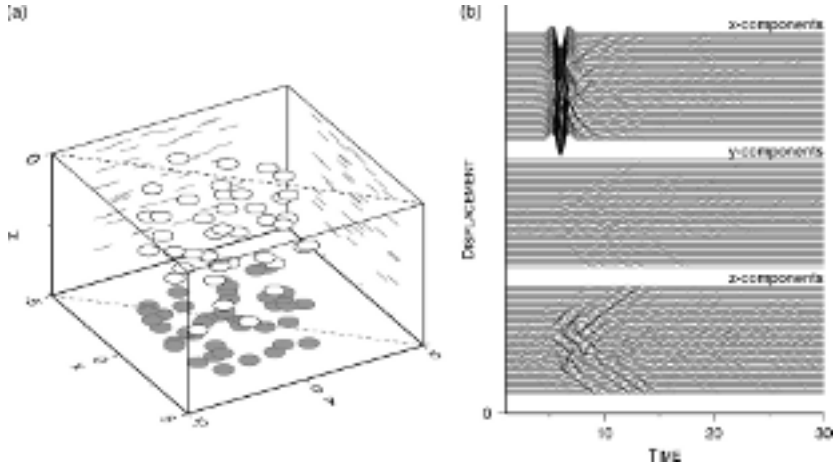


**Figure 15.** (a) Distribution of 40 passive cracks in infinite elastic medium. (b) Calculated displacements at the observation points on the profile line.

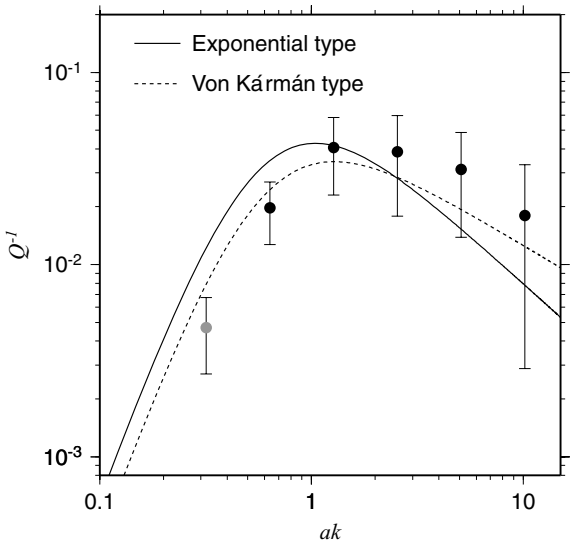


**Figure 16.** Scattering attenuation $Q^{-1}$ as a function of $ak$. The 25 passive cracks of radius $a$ in Fig. 12 are used for the calculations, by changing dominant wavenumber $k$ of incident wave. For $ak = 0.32$, 0.64, 1.27, 2.54, 5.08 and 10.2, the averages of $Q^{-1}$ and their standard deviations are indicated by solid circles and error bars. Solid and broken curves are calculated by single scattering models (Wu 1982) with rms velocity variation of 40 per cent. The exponential and Von Kármán type auto correlation functions of velocity variation are used in this calculation.

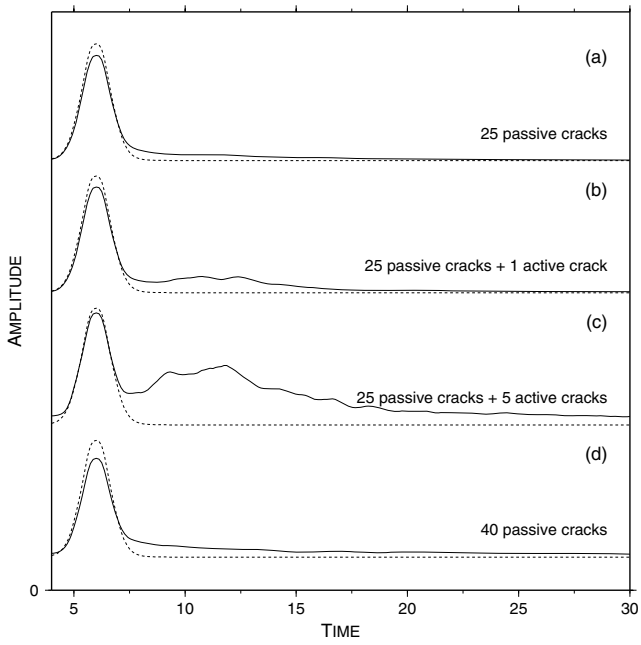


**Figure 17.** The rms envelopes for four models (solid lines). For each model, the envelopes of velocity waveforms are calculated for the 441 equally spaced points at the indicated plane $z = 0$ (Figs 12, 14a, 15a). Broken line is the envelope of incident wave. (a) 25 passive cracks, (b) 25 passive cracks and one active crack, (c) 25 passive cracks and 5 active cracks, (d) 40 passive cracks.

coda. Some peaks seen in the envelopes for the models containing the active cracks are mainly the radiated waves from the rupture of the active cracks (Figs 17b and c). These results indicate the importance of the active cracks: they can produce additional coda waves from the energy radiation due to rupture, while the amplitude of the first arrival from incident wave may scarcely attenuate regardless of the number of the active cracks because the attenuation of direct wave is mainly associated with the scattering by the passive cracks.

## 4 DISCUSSION

### 4.1 Numerical results

The coda waves in the structure with active cracks show large amplitudes, which agree with the fact that the active cracks radiate internal strain energy. Another property is the slow decay of coda amplitude. This can be derived by measuring coda attenuation $Q_C^{-1}$ of $ak \sim 1$ for each model in Fig. 17. Ratios of coda attenuation for the four models with plane-wave incidence are $Q_C^{-1}$ (a):$Q_C^{-1}$ (b):$Q_C^{-1}$ (c):$Q_C^{-1}$ (d) = 1.00:0.92:0.45:0.68, where we take the time-window 20–30, and in which (a)–(d) correspond to the models of Figs 17(a)–(d), respectively. The coda attenuation factor $Q_C^{-1}$ decreases with the number of passive or active cracks. The active cracks make slower the decay of the coda wave amplitudes than the passive crack, possibly due to the strong multiple scattering around the active cracks. The passive cracks surrounding the active cracks make it difficult that the propagation of the waves radiated by their rupture. Scattered waves are influenced by the mean distribution of cracks, while the radiated waves from the active cracks are affected by the distribution of the

neighbouring cracks. The relative locations of the active and passive cracks are important.

Only one random realization is assumed in this paper, but we have confirmed that other random realizations also generate similar wavefields, as long as the size and density of the cracks are not changed. Similar rms envelopes are obtained for the models of the passive cracks as shown in Figs 17(a) and (d). However, if we assume different locations of the active cracks, the coda waves observed at the stations could be different.

### 4.2 Realistic model and actual structure

We choose an *S* wave as the incident wave, but an active crack can be as well excited by the incidence of a *P* wave or a surface wave. In any case, the relation between the incident direction of the wave and normal vector of the boundary of the active crack is important for dynamic triggering and scattering. Considering the cracks around a fault zone (Reches & Lockner 1994; Vermilye & Scholz 1998; Yamashita 2000), a realistic model should incorporate not only with horizontal cracks but also with oblique cracks, where the properties of the active cracks reflecting surrounding stress field should be investigated as well as the main fault.

When the medium contains many cracks to represent realistic structures, the numerical computations even by BIEM become tremendous. In case of the large number of boundaries, fast multipole method (e.g. Fujiwara 2000) is useful for calculating multiple scattering of waves between the active and the passive cracks.

The rupture of the active crack starts when the stress reaches the yield stress, while the rupture start becomes possible when the yield stress drops to the initial stress (e.g. Kilb *et al.* 2000). Also low-frequency components of incident waves have potential abilities to trigger the crack as well as the large amplitude (e.g. Gomberg *et al.* 1997; Voisin 2002).

We must take account of the intrinsic attenuation, which might play a more important role in the amplitude variations of observed seismic waves than the scattering attenuation. The observed waveforms are influenced by three factors: intrinsic attenuation, scattering attenuation and seismic radiation from the active structure. The first two attenuation factors are measured from observations (e.g. Hoshiba 1993). The complicated combination of these three factors seems to make it difficult to detect the evidence of the active structure.

At shallow volcanic and geothermal regions, the active structure is actually found. For example, teleseismic waves from large earthquakes triggered frequent volcanic tremors and microearthquakes, which could slightly increase the amplitude of the coda (Miyazawa *et al.* 2005). Hence, as far as the sources in the active structure locate in shallow region and we are capable of recording the signals with good S/N ratios, the actual observation of specific coda predicted in this study would be potentially possible.

## 5 CONCLUSIONS

BIEM is applied to the calculations of the wave scattering in idealized models of passive and active structures. The passive structure is modelled by passive (open) cracks in a 3-D elastic medium, and the active structure by passive and active (closed) cracks. The passive cracks decrease the amplitude of incident wave by scattering, and the multiply scattered waves are observed in coda. The active cracks are dynamically triggered by incident waves, the total energy of the wavefield increases due to the radiation of elastic waves from the active cracks, and multiple scattering with slowly decaying high amplitude is observed in coda waves.

The lithosphere would consist of the passive and active structures, therefore, observed seismic waves are affected by intrinsic absorption, scattering attenuation and probably negative attenuation due to the dynamic triggering. We should take account of not only the attenuation but also the negative attenuation, if the structure seems to be active.

## ACKNOWLEDGMENTS

This study was supported by a research grant of Japan Society for the Promotion Science research fellowships for younger scientists, the Kurata Memorial Hitachi Science and Technology Foundation and the Earthquake Research Institute cooperative research program. We used the Generic Mapping Tools (Wessel & Smith 1998) to illustrate figures. We appreciate the comments from two anonymous reviewers, and the editor, Dr A. J. Haines.

## REFERENCES

Achenbach, J.D., Gautesen, A.K. & McMaken, H., 1982. *Ray Methods for Waves in Elastic Solids: with Applications to Scattering by Cracks*, Pitman Advanced Pub., Boston, p. 251.

Andrews, D.J., 1976. Rupture velocity of plane strain shear cracks, *J. geophys. Res.,* **81,** 5679–5687.

Aochi, H., Madariaga, R. & Fukuyama, E., 2002. Effect of normal stress during rupture propagation along nonplanar faults, *J. geophys. Res.,* **107**, doi:10.1029/2001JB000500.

Beskos, D.E. ed., 1987. *Boundary Element Methods in Mechanics*, North-Holland, Amsterdam, p. 598.

Dahlen, F.A., 1974. On the ratio of *P*-wave to *S*-wave corner frequencies for shallow earthquake sources, *Bull. seism. Soc. Am.,* **64,** 1159–1180.

Das, S., 1980. A numerical method for determination of source time functions for general three-dimensional rupture propagation, *Geophys. J. R. astr. Soc.,* **62,** 591–604.

Das, S. & Kostrov, B.V., 1987. On the numerical boundary integral equation method for three-dimensional dynamic shear crack problems, *J. Appl. Mech.,* **54,** 99–104.

Diakonov, B.P., Karryev, B.S., Khavroshkin, O.B., Nikolaev, A.V., Rykunov, L.N., Seroglasov, R.R., Trojanov, A.K. & Tsyplakov, V.V., 1990. Manifestation of earth deformation processes by high-frequency seismic noise characteristics, *Phys. Earth planet. Inter.,* **63,** 151–162.

Eringen, A.C. & Suhubi, E.S., 1975. *Elastodynamics*, **2**, Academic Press, New York.

Everett, M.E., 1997. A three-dimensional spherical mesh generator, *Geophys. J. Int.,* **130,** 193–200.

Frankel, A. & Clayton, R.W., 1986. Finite difference simulations of seismic scattering: implications for the propagation of short-period seismic waves in the crust and models of crustal heterogeneity, *J. geophys. Res.,* **91,** 6465–6489.

Fujiwara, H., 2000. The fast multipole method for solving integral equations of three-dimensional topography and basin problems, *Geophys. J. Int.,* **140,** 198–210.

Fukuyama, E. & Madariaga, R., 1998. Rupture dynamics of a planar fault in a 3D elastic medium: rate- and slip-weakening friction, *Bull. seism. Soc. Am.,* **88,** 1–17.

Galperin, E.I., Petersen, N.V., Sitnikov, A.V. & Vinnik, L.P., 1990, On the properties of short-period seismic noise, *Phys. Earth planet. Inter.,* **63,** 163–171.

Gomberg, J., Blanpied, M.L. & Beeler, N.M., 1997. Transient triggering of near and distant earthquakes, *Bull. seism. Soc. Am.,* **87,** 294–309.

Harris, R.A., 1998. Introduction to special section: stress triggers, stress shadows, and implications for seismic hazard, *J. geophys. Res.,* **103,** 24 347–24 358.

Hill, D.P. et al., 1993. Seismicity remotely triggered by the magnitude 7.3 Landers, California, earthquake, *Science,* **260,** 1617–1623.

Hoshiba, M., 1993. Separation of scattering attenuation and intrinsic absorption in Japan using the multiple lapse time window analysis of full seismogram envelope, *J. geophys. Res.,* **98,** 15 809–15 824.

Iwata, T. & Nakanishi, I., 2004. Hastening of occurrences of earthquakes due to dynamic triggering: The observation at Matsushiro, central Japan, *J. Seism.,* **8,** 165–177.

Kame, N. & Yamashita, T., 1999. Simulation of the spontaneous growth of a dynamic crack without constraints on the crack tip path, *Geophys. J. Int.,* **139,** 345–358.

Kawahara, J. & Yamashita, T., 1992. Scattering of elastic waves by a fracture zone containing randomly distributed cracks, *Pure. appl. Geophys.,* **139,** 121–144.

Kilb, D., Gomberg, J. & Bodin, P., 2000. Triggering of earthquake aftershocks by dynamic stresses, *Nature,* **408,** 570–574.

Kitahara, M., 1985. *Boundary Integral Equation Methods in Eigenvalue Problems of Elastodynamics and Thin Plates*, Elsevier, Amsterdam, p. 281.

Kobayashi, S., 1987. Elastodynamics, In: *Boundary Element Methods in Mechanics*, ed. Beskos, D.E., North-Holland, Amsterdam, Chap. 4, 192–255.

Kobayashi, S. ed., 2000, *Wave Analysis and Boundary Element Method*, Kyoto Univ. Press, Kyoto, p. 338, in Japanese.

Kupradze, V.D. ed., 1979, *Three-dimensional Problems of the Mathematical Theory of Elasticity and Thermoelasticity*, North-Holand Publ. Co., Amsterdam.

Martin, P.A. & Wickham, G.R., 1983. Diffraction of elastic waves by a penny-shaped crack: analytical and numerical results, *Proc.R. Soc. London Ser.,* A **390,** 91–129.

Miyazawa, M. & Mori, J., 2005. Detection of triggered deep low-frequency events from the 2003 Tokachi-oki earthquake, *Geophys. Res. Lett.,* **32,** L10307, doi:10.1029/2005GL022539.

Miyazawa, M., Nakanishi, I., Sudo, Y. & Ohkura, T., 2005. Dynamic response of frequent tremors at Aso volcano to teleseismic waves from the 1999 Chi-Chi, Taiwan earthquake, *J. Volcanol. Geotherm. Res.,* **147,** 173–186.

Murai, Y., Kawahara, J. & Yamashita, T., 1995. Multiple scattering of *SH* waves in 2-D elastic media with distributed cracks, *Geophys. J. Int.,* **122,** 925–937.

Nikolaev, A.V. & Troitskiy, P.A., 1987. Lithospheric studies based on array analysis of *P*-coda and microseisms, *Tectonophysics,* **140,** 103–113.

Nishimura, N. & Kobayashi, S., 1987. On the behavior of elastic potentials, *Mem. Fac. Eng. Kyoto Univ.,* **49,** 294–307.

Nishimura, N. & Kobayashi, S., 1989. A regularized boundary integral equation method for elastodynamic crack problems, *Comp. Mech.,* **4,** 319–328.

Pao, Y.H. & Mow, C.C., 1973. *Diffraction of Elastic Waves and Dynamic Stress Concentrations*, Crane-Russak, New York, p. 694.

Privalovskiy, N.K. & Beresnev, I.A., 1994. Seismic noise emission induced by seismic waves, *Geophys. J. Int.,* **116,** 806–812.

Reches, Z. & Lockner, D.A., 1994. Nucleation and growth of faults in brittle rocks, *J. geophys. Res.,* **99,** 18 159–18 173.

Richards, P.G., 1973. The dynamic field of a growing plane elliptical shear crack, *Int.J. Solids Structures,* **9,** 843–861.

Ricker, N., 1945. The computation of output disturbances from amplifiers for true wavelet inputs, *Geophysics,* **10,** 207–220.

Rykunov, L.N., Khavroshkin, O.B. & Tsyplakov, V.V., 1979. Time variations of high-frequency seismic noise, *Izvestiya, Earth Physics,* **15,** 829–833.

Sato, T., 1994. Seismic radiation from circular cracks growing at variable rupture velocity, *Bull. seism. Soc. Am.,* **84,** 1199–1215.

Sato, H. & Fehler, M., 1998. *Seismic Wave Propagation and Scattering in the Heterogeneous Earth*, Springer, New York, p. 308.

Sato, T. & Hirasawa, T., 1973. Body wave spectra from propagating shear cracks, *J. Phys. Earth,* **21,** 415–431.

Tanaka, M., Sladek, V. & Sladek, J., 1994. Regularization techniques applied to boundary element methods, *Appl. Mech. Rev.,* **47,** 457–499.

Vermilye, J.M. & Scholz, C.H., 1998. The process zone: A microstructural view of fault growth, *J. geophys. Res.,* **103,** 12 223–12 237.

Vinnik, L.P., 1989. Seismic emission and seismic holography, *Izvestiya, Earth Physics,* **8,** 108–111.

Voisin, C., 2002. Dynamic triggering of earthquakes: The nonlinear slip-dependent friction case. *J. geophys. Res.,* **107**, doi:10.1029/2001JB001121.

Wessel, P. & Smith, W.H.F., 1998. New, improved version of Generic Mapping Tools released, *EOS, Trans. Am. geophys. Un.,* **79,** 579.

Wu, R.S., 1982. Attenuation of short period seismic waves due to scattering, *Geophys. Res. Lett.,* **9,** 9–12.

Yamashita, T., 2000. Generation of microcracks by dynamic shear rupture and its effects on rupture growth and elastic wave radiation, *Geophys. J. Int.,* **143,** 395–406.

Yomogida, K. & Benites, R., 1995. Relation between direct wave *Q* and coda *Q*: a numerical approach, *Geophys. J. Int.,* **123,** 471–483.

Yomogida, K. & Benites, R., 2002. Scattering of seismic waves by cracks with the boundary integral method, *Pure. appl. Geophys.,* **159,** 1771–1789.